Geophys. J. R. astr. Soc. (1980) **62**, 195–219

A boundary layer model for mantle convection with surface plates

Peter Olson *Department of Earth and Planetary Sciences, Johns Hopkins University, Baltimore, Maryland 21218, USA*

G. M. Corcos *Department of Mechanical Engineering, University of California, Berkeley, CA 94720, USA*

Received 1979 November 19; in original form 1979 June 11

Summary. A simple, analytical model for mantle convection with mobile surface plates is presented. Our aim is to determine under what conditions free convection can account for the observed plate motions, and to evaluate the thermal structure of the mantle existing under these conditions. Boundary layer methods are used to represent two-dimensional cellular convection at large Rayleigh and infinite Prandtl numbers. The steady-state structure consists of cells with isentropic interiors enclosed by thermal boundary layers. Lithospheric plates are represented as upper surfaces on each cell free to move at a uniform speed. Buoyancy forces are concentrated in narrow rising and decending thermal plumes; torques imparted by these plumes drive both the deformable mantle and overlying plate. Solutions are found for a comprehensive range of cell sizes. We derive an expression for the plate speed as a function of its length, the mantle viscosity and surface heat flux. Using mean values for these parameters, we find that thermal convection extending to 700 km depth can move plates at 1 cm yr^{-1}, while convection through the whole mantle can move plates at 4–5 cm yr^{-1}. Analysis of the steady-state temperature field, for the case of heating from below, shows that the upper thermal boundary layer develops a complex structure, including an 'asthenosphere' defined by a local maximum in the geotherm occurring at depths of 50–150 km.

1 Introduction

We present here an analytical, boundary layer theory to describe the interaction of mantle convection with surface plates. Our chief purpose is to address the following question: Can lithospheric plates be moved at their observed speeds by the action of mantle convection? It seems that past studies have not paid sufficient attention to this question, and this is perhaps partly responsible for the current lack of agreement on the rôle played by free convection in plate tectonics.

Faced with phenomena as complex as plate motions, it is not possible for any individual study to explain all observations or to include all possible complicating effects. With these limitations in mind, we restrict attention to the question of whether mantle convection can reasonably achieve the surface speeds and stresses to move the plates. Boundary layer theory is in some respects well suited to this task since it becomes an increasingly accurate approximation in the limit of large Rayleigh numbers, and it is in this limit that substantial convective velocities occur.

On the other hand, an analytical approach restricts consideration to very idealized conditions; namely steady-state, two-dimensional flows with constant transport properties. Nevertheless, with the boundary layer formulation this ideal case can be analysed so succinctly that we are encouraged to think that it can be profitably used on more elaborate two-dimensional and even three-dimensional problems.

The plan of this presentation is as follows: Section 2 is devoted to a review of previous work, Section 3 gives a physical description of the problem, in Sections 4 and 5 the velocity and temperature fields are found, in Section 6 these two fields are matched and Section 7 presents the main results as well as a brief discussion of the thermal structure of the mantle in light of these results.

The analysis is confined to Sections 4–6, so the reader not interested in all details may pass quickly over these sections.

2 Previous work

Foundations for the boundary layer approach were first developed by Turcotte & Oxburgh (1967); see also Turcotte (1967). This work demonstrated that for steady cellular convection in a horizontal layer at large Rayleigh numbers each cell develops an isothermal core surrounded by thin thermal boundary layers. As long as the transport properties remain constant, the convection is simply a Stokes flow driven by buoyancy of the thermal layers. Turcotte & Oxburgh presented a simplified analysis of the problem, which among other things ignored the heat transferred by buoyant plumes, and which treated the upper surface as a free boundary. Later, Robinson (1967) presented an improved version of the boundary layer structure, but did not carry through a complete calculation of the flow at infinite Prandtl number, which is the limit of interest in mantle dynamics.

Since then, the emphasis has been on numerical finite difference methods which have the capability of including three space dimensions, time dependence as well as variable transport properties.

Moore & Weiss (1973) performed numerical experiments on convection driven by heat supplied from below in square domains over a wide range of Prandtl numbers. At infinite Prandtl number, they obtained steady solutions for Rayleigh numbers up to $\simeq 10^6$ which represented roughly the limiting value of this parameter imposed by their choice of grid size. *Extensive calculations on the same domain were carried out by McKenzie, Roberts & Weiss* (1974).

Both of the above studies included free upper boundaries plus constant transport properties with the result that the upper surface of each cell did not behave like a plate. The presence of plates, that is an upper surface which moves with a piece-wise constant velocity, is an essential feature of mantle convection, and there have been numerous investigations which in one way or another have sought to incorporate this. Houston & DeBremacker (1975) studied convection in layers with strongly temperature and pressure dependent viscosity. While the variable viscosity strongly affected the flow (for example they obtained

the surprising result that elongated cells with aspect ratios up to 8.6 were stable), the upper surface did in no case become a moving plate. Evidently the existence of moving, discrete plates implies a complicated rheological behaviour that is not justifiably represented by viscosity alone, even if it is dependent on state variables. The rheological contrast between the plates and underlying mantle also means among other things that the stability of a particular configuration of trenches and ridges is not wholly a fluid mechanics problem. Though this point has long been recognized, most geophysicists are still inclined to use results from the theory of thermal instability in homogeneous layers to predict the scales of motion, simply because of a lack of alternatives.

Recently there have been some attempts to include effects of this inhomogeneity by representing plate motions as a kinematic condition along the upper surface of the convecting domain. Parmentier & Turcotte (1978) investigated, numerically, convection beneath a uniformly translating upper boundary. They found that for even small rates of translation and vigorous heating, the circulation is dominated by the moving boundary, and that smaller scale flows driven by interior buoyancy play a secondary rôle. One difficulty in interpreting these results is the fact that the surface velocity is externally prescribed rather than determined by the energetics of a closed system. In this paper, the deformable mantle and overlying plate will be taken to be a single system and the plate motion will be a result of interior, thermally induced buoyancy forces. This point of view is similar to that adopted by Lux, Davies & Thomas (1979) who used numerical methods to determine translation speeds for a free drifting plate overlying a convecting layer.

Finally, we note that there has been some initial work on the very difficult problem of three-dimensional convection in a spherical domain (Schubert & Young 1976). At least in principle, the methods developed in the present study can be extended to three-dimensional flows.

A limitation in all the above mentioned finite difference approaches is that at large Rayleigh numbers the temperature field becomes confined to thin layers which are not adequately resolved by a uniform mesh. This problem is avoidable using boundary layer analysis, in which the heat and momentum equations are solved over separate domains, and their solutions can be matched by simple quadrature. The methods we develop here are an improvement upon the coarse approximations used by Turcotte & Oxburgh. We derive analytic expressions for temperature and velocity fields, and present solutions for a wide range of cell sizes. In principle, the accuracy of this method is limited only by the approximations of boundary layer theory. Numerical results for viscous Bénard convection using boundary layer approximations are given by Roberts (1979), and our analytical results agree with his in order of magnitude.

3 Formulation of problem

The system to be considered is a layer of fluid with infinite Prandtl number bounded by horizontal surfaces $Z = 0, D$ which are kept at temperatures T_0 and T_1 respectively. We will investigate steady motions in the form of two-dimensional rolls of width ΔD, arranged periodically in the X direction (see Fig. 1).

By choice, the lower boundary is taken to be stress free; other conditions are easily handled. Because of low temperatures, the upper surface remains undeformed and is free to move only at a constant speed. The speed is determined by specifying the net shear stress on the plate: in this work we take the plate to be horizontal with no net stress acting on it; however, applied net stresses can be included if desirable. Because of its simplicity, we will mainly be concerned with convection in the absence of internal heat sources, in which case

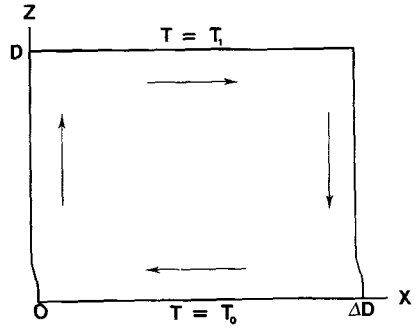

Figure 1. Coordinate system used in analysis, with upper and lower surfaces kept at temperatures T_1 and T_0, respectively. Circulation is clockwise.

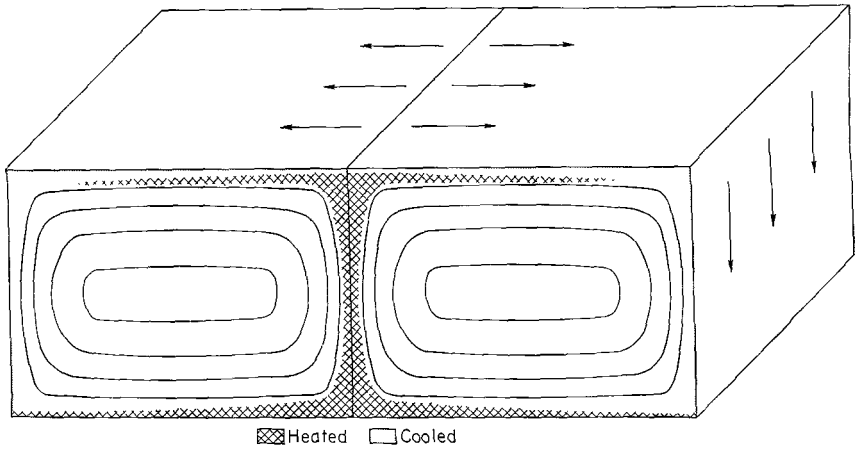

Figure 2. Sketch of circulation showing streamlines plus hot and cold thermal boundary layers and plumes.

the heat flux across the lower surface equals the flux across the upper one. In addition to the results with a moving plate, we include the solution for convection in a homogeneous fluid with both boundaries stress free (the Rayleigh–Bénard problem). This allows comparison between our asymptotic results and numerical simulations carried out at large but finite Rayleigh numbers.

Fig. 2 is a sketch of the interior structure when all heat is supplied from below. At large Rayleigh numbers, all heat entering through the lower boundary is swept into a thin thermal boundary layer and delivered to thermal plumes which form along vertical planes between cells. Throughout we refer to the vertical thermal layers as 'plumes', the horizontal thermal layers are simply called 'boundary layers'. Since all the heat is transported within thermal boundary layers, the circulating mantle material enclosed within the layers is shielded from temperature fluctuations, and with time any existing non-adiabatic temperature anomalies become reduced by diffusion. In steady state, the interior is isentropic. The temperature field in the boundary layers is best understood by following a small control volume of the boundary layer material. As it circulates about the cell it is alternatingly heated at the lower surface, cooled at the upper one, and insulated in the plumes. Hence the parcel is subjected to periodically varying temperatures at its outer edge; the resulting temperature profile is oscillatory with an exponentially decreasing amplitude away from the cell edge.

To a good approximation, the behaviour can be represented as follows. The ascending plume arrives at the upper surface, and spreads out to form a hot layer between the cold

material immediately adjacent to the free surface and the warm, isentropic interior. This hot layer is defined by a local maximum in the boundary layer temperature profile. As Fig. 2 indicates, the hot layer gradually erodes downstream so that the boundary layer becomes very nearly (but not exactly) self-similar as it approaches the descending plume. The lower layer has structure conjugate to the upper one. In this arrangement, all buoyancy is concentrated in narrow plumes, and the entire flow is a two-dimensional Stokes flow driven at its edges by buoyancy forces.

If all heat is produced by internal volumetric sources, there is no ascending plume and no hot layer below the upper surface. In place of the ascending plume is a broad ascending region extending over most of the cell, and in this case the interior is no longer adiabatic: a small subadiabatic gradient develops as the plume material becomes reheated during its gradual ascent.

Since we fix the plume positions and assume a steady state, we cannot decide exactly which cell sizes are stable and which are unstable. The question of stability in subsolidus convection has proven to be troublesome, largely because we lack an adequate rheological description for surface plates. However, we find that the behaviour of the lower boundary layer can be used as a stability criteria since its thickness and hence its stability depends strongly on the width of the cell.

Finally, we note that the choice of rectangular shaped cells is a matter of convenience. It is a straightforward matter to apply this analysis to a cylindrical annular domain; this would simulate the effects of curved level surfaces; for instance the plates would then move with constant angular velocities.

4 Equations of motion; the stream-function

In this section the stream-function for the flow is obtained. The equations of motion, with Boussinesq approximation are

$$\frac{d}{dt}\mathbf{u} = -1/\rho_m \nabla P_1 + \alpha g \hat{z}\theta + \nu\nabla^2\mathbf{u} \tag{1a}$$

$$\nabla\cdot\mathbf{u} = 0 \tag{1b}$$

$$\frac{d\theta}{dt} = k\nabla^2\theta + H. \tag{1c}$$

Here $\mathbf{u}(=\hat{x}u + \hat{z}W)$ is velocity, P_1 is reduced pressure, α is thermal expansion, g is acceleration of gravity, ν is kinematic viscosity, k is thermal diffusivity, H is specific heat source density, ρ_m is mean density, and

$$\theta = T - \frac{(T_0 + T_1)}{2}$$

is the deviation of temperature from its mean value.

The boundary conditions on horizontal surfaces are

$$W = \partial u/\partial z = 0, \qquad \theta = \frac{T_0 - T_1}{2} = \frac{\Delta T}{2} \qquad \text{on } Z = 0, \tag{2a}$$

$$W = \langle \partial u/\partial z \rangle = 0, \qquad \theta = -\Delta T/2 \qquad \text{on } Z = D, \tag{2b}$$

where $\langle\ \rangle$ denotes horizontal average. For the case of a homogeneous fluid, with no surface plate, the boundary condition (2b) becomes

$$W = \frac{\partial u}{\partial z} = 0 \qquad \text{on } Z = D. \tag{2c}$$

For both cases, we have

$$u = 0 \qquad \text{on } X = 0, \Delta D. \tag{2d}$$

Turcotte & Oxburgh (1967) and Roberts (1977) have shown that these conditions may be applied directly to the interior flow. The remaining, non-homogeneous conditions will be derived later in this section.

In distinguishing between dimensional and dimensionless variables, the following notation convention is adhered to. Initially, we define non-dimensional variables with asterisks; this convention is dropped when the non-dimensional equations have been formulated, since non-dimensional equations are dealt with exclusively throughout the remainder of this section and the next one. However, the final parts, Sections 7–8, include discussion of formulae with both dimensional and non-dimensioned variables, and there we return to the convention of denoting dimensionless quantities with asterisks.

Our choice of scaling is such as to make the velocity $O(1)$ throughout the domain.

Let

$$\mathbf{X} = DX^*$$

$$\mathbf{u} = u_0\mathbf{u}^*, \qquad \text{where } u_0 = kR^{2/3}/D \tag{3}$$

$$P_1 = \frac{\rho_m \nu u_0}{D} P_1^*$$

$$\theta = \Delta T\theta^*$$

$$H = \frac{k\Delta TR^{1/3}}{D^2} H^*$$

where C_p is specific heat, and R is the Rayleigh number, defined below. With these the equations of motion (1) become

$$\frac{R^{2/3}}{Pr}\frac{d}{dt^*}\mathbf{u}^* = -\nabla^* P_1^* + R^{1/3}\theta^*\hat{z} + \nabla^{*2}\mathbf{u}^* \tag{4a}$$

$$\nabla^* \cdot \mathbf{u}^* = 0 \tag{4b}$$

$$\frac{d}{dt^*}\theta^* = \frac{1}{R^{2/3}}\nabla^{*2}\theta^* + H^*/R^{1/3} \tag{4c}$$

where $Pr = \nu/k$ is the Prandtl number, and

$$R = \frac{\alpha g D^3}{k\nu}\Delta T$$

is the Rayleigh number. The Boussinesq approximation we have adopted here is valid if the dissipation number $Di = \alpha gD/C_p$ is less than unity (Turcotte *et al.* 1974). Using values

from Table 2, we have $Di \approx 1/3$ for $D = 2900$ km, so that this approximation is at least formally valid. This is helpful because it allows us to carry out the computation assuming incompressibility, and then simply add adiabatic increases to our computed temperature profiles to produce model geotherms. With the Boussinesq approximation, and the effectively infinite Prandtl number (for the mantle $Pr \approx 10^{24}$, so the left-hand side of equation (4a) is negligible) only two parameters are left: R and the cell width Δ. All variables can be expressed in terms of these two quantities.

Note that the energy equation (4c) is scaled on the layer depth D. This is not appropriate within the thermal layers since there the conductive and advective terms must be of the same order. These two terms balance in the thermal layers only if the boundary layer thickness δ is $O(DR^{-1/3})$, or in dimensionless terms, $\delta^* \sim R^{-1/3}$. This means that the Nusselt number is

$$Nu \sim 1/\delta^* \sim R^{1/3}.$$

Our scaling then yields the following two functional relationships

$$Nu = qD/K\Delta T = a_1(\Delta)R^{1/3} \tag{5a}$$

$$V = a_2(\Delta)\frac{k}{D}R^{2/3} \tag{5b}$$

where V is the plate speed, q is surface heat flux and K is thermal conductivity and a_1, a_2 are geometrical factors. These two may be usefully combined to eliminate the temperature increment ΔT (Elsasser, Olson & Marsh 1979). The result is an expression for the plate velocity in terms of the convecting layer thickness and some geophysically measurable parameters:

$$V = \frac{a_2}{a_1^{1/2}}\left(\frac{\alpha g}{C_p}\right)^{1/2}(q/\mu)^{1/2}D. \tag{6}$$

Here μ is dynamic viscosity, and the factors a_1 and a_2 are functions of the cell aspect ratio Δ which will be determined in the subsequent analysis. Use of formula (6) is made in Section 7.

It is important to note that the Rayleigh and Nusselt numbers as defined here play different rôles depending on whether the heat is generated internally or supplied from below. For the case of heating from below, R is fixed and Nu depends on it, but if all heat is internally generated q is fixed while ΔT, the temperature rise across the layer and hence R are variable.

Now it is possible to derive the remaining, non-homogeneous boundary conditions which are to be applied along vertical edges of the cell. Let γ be that fraction of the heat carried by the plume at $X = 0$; when heat is supplied entirely from below $\gamma \simeq 1/2$. The heat transferred by both plumes may be equated to the heat entering or leaving the cell to yield

$$W^* \int_0^{\delta_p^*} (\theta^* - \theta_i^*)\, dX^* = \frac{\gamma Nu \Delta}{R^{2/3}} \tag{7}$$

δ_p^* being the plume thickness, and θ_i^* the temperature in the cell's interior. Within the plumes, the momentum equation (4a) can be integrated once to yield

$$\left.\frac{\partial W^*}{\partial X^*}\right|_{X^* = \delta_p^*} = -R^{1/3}\int_0^{\delta_p^*} (\theta^* - \theta_i^*)\, dX^*. \tag{8}$$

In the limit $R \to \infty$, $\delta_p^* \to 0$, in which case equations (7) and (8) combine to yield

$$W^* \frac{\partial W^*}{\partial X^*} = -\frac{\gamma \Delta Nu}{R^{1/3}} \qquad \text{at } X^* = 0 \tag{9}$$

$$= \frac{(1-\gamma)\Delta Nu}{R^{1/3}} \qquad \text{at } X^* = \Delta.$$

These non-homogeneous boundary conditions determine the interior flow.

Equation (8) implies that each plume acts as a source of vorticity whose strength is $O(1)$. This vorticity can be compared with vorticity induced by temperature anomalies in the cell interior. When R is large, and away from boundaries, equation (4c) reduces to

$$\frac{d\theta^*}{dt^*} = 0 \tag{10}$$

or

$$\theta^* = \theta^*(\psi^*) \tag{11}$$

ψ^* being the stream-function. Because of the boundary conditions on temperature (equations 2), θ^* approaches a constant in the interior, θ_i^*. Referring to equation (4c), the interior is isentropic to $O(R^{-2/3})$ for heat from below, and is isentropic to $O(R^{-1/3})$ for heat generated internally. The curl of equation (4a) yields

$$\nabla^{*2}\omega^* = R^{1/3} \frac{\partial \theta^*}{\partial X^*} \tag{12}$$

where ω^* is vorticity. When the heating is from below, the right-hand side of equation (12) vanishes to $O(R^{-1/3})$ and plume sources of vorticity are large compared with internal sources. If all heat is produced internally, then the right-hand side of equation (12) vanishes to $O(1)$ in which case the plumes and interior contribute to the vorticity in roughly equal amounts, and the boundary layer method breaks down.

Thus for heating from below only, equation (12) reduces to

$$\nabla^{*2}\omega^* = \nabla^{*4}\psi^* = 0 \tag{13}$$

where ψ^* is defined by $\mathbf{u}^* = -\hat{y} \times \nabla^* \psi^*$ and the flow governed by equation (13) is driven by the plumes' buoyancy as expressed in equation (9). This analysis indicates that in the presence of internal heat sources, the flow cannot be accurately computed by considering buoyancy forces in the plumes only. For basal heating, the problem is now reduced to a Stokes flow subject to boundary data which are expressed in terms of the surface heat flux. From equations (2), (9) and (13) we have (dropping the asterisk notation now that the problem is formulated in dimensionless terms)

$$\nabla^4 \psi = 0 \tag{14}$$

subject to

$$\psi = 0 \qquad \text{on } Z = 0, 1, \tag{15a}$$

$$\psi = 0 \qquad \text{on } X = 0, \Delta, \tag{15b}$$

$$\frac{\partial^2 \psi}{\partial Z^2} = 0 \qquad \text{on } Z = 0, \tag{15c}$$

$$\frac{\partial \psi}{\partial Z} = \text{constant} \qquad \text{on } Z = 1, \tag{15d}$$

$$\left\langle \frac{\partial^2 \psi}{\partial Z^2} \right\rangle = 0 \qquad \text{on } Z = 1, \tag{15e}$$

$$\frac{\partial \psi}{\partial X}\frac{\partial^2 \psi}{\partial X^2} = \frac{-\gamma \Delta Nu/R^{1/3}}{(1-\gamma)\Delta Nu/R^{1/3}} \qquad \text{on } X = \begin{matrix} 0 \\ \Delta \end{matrix}. \tag{15f}$$

The general solution to equation (14) in a rectangular domain is

$$\psi = F_1(X+iZ) + F_2(X-iZ) + (Z+iX)F_3(X+iZ) + (Z-iX)F_4(X-iZ)$$

where F_1–F_4 are arbitrary functions of their arguments. A solution which satisfies equation (15a–e) is

$$\psi = \psi_f + \psi_p,$$

$$\psi_f = \frac{\Delta}{2}\sum_{n=1}^{\infty}\left(\frac{\sin n\pi Z}{n^2\pi^2}\right)\left\{(B_n + D_n)\left[\frac{\cosh \beta_n - [(X-\Delta/2)\cosh \alpha_n \sinh \beta_n]/(\Delta/2 \sinh \alpha_n)}{\cosh \alpha_n \operatorname{ctnh} \alpha_n}\right]\right.$$
$$\left. + (B_n - D_n)\left[\frac{\sinh \beta_n - [(X-\Delta/2)\sinh \alpha_n \cosh \beta_n]/(\Delta/2 \cosh \alpha_n)}{\tanh \alpha_n \sinh \alpha_n}\right]\right\}$$

$$\psi_p = \sum_n A_n [\sinh \omega_n Z - Z \tanh \omega_n \cosh \omega_n Z] \sin \omega_n X \tag{16}$$

where

$$\alpha_n = \frac{n\pi\Delta}{2}, \qquad \omega_n = n\pi/\Delta, \qquad \beta_n = n\pi(X - \Delta/2)$$

$$A_n = \frac{4M}{n\pi P_n} - \frac{2I_n}{\Delta P_n}$$

$$I_n = \int_0^{\Delta} \left.\frac{\partial \psi_f}{\partial Z}\right|_{Z=1} \sin \omega_n X \, dX$$

$$P_n = \sinh \omega_n(1 + \omega_n \tanh \omega_n) - \omega_n \cosh \omega_n$$

$$q_n = \left(\frac{4\Delta}{n\pi}\right)\omega_n \sinh \omega_n \tanh \omega_n$$

$$M = \frac{\sum_{n=1}^{\infty} \frac{I_n q_n}{\Delta P_n}}{\sum_{n=1}^{\infty} \frac{2q_n}{n\pi P_n}}.$$

The coefficients B_n and D_n are available to satisfy the remaining two conditions (15f).

The full solution, $\psi = \psi_f + \psi_p$ is the stream-function when a surface plate is present. The first term only, $\psi = \psi_f$ is the stream-function for a homogeneous fluid bounded by two free surfaces.

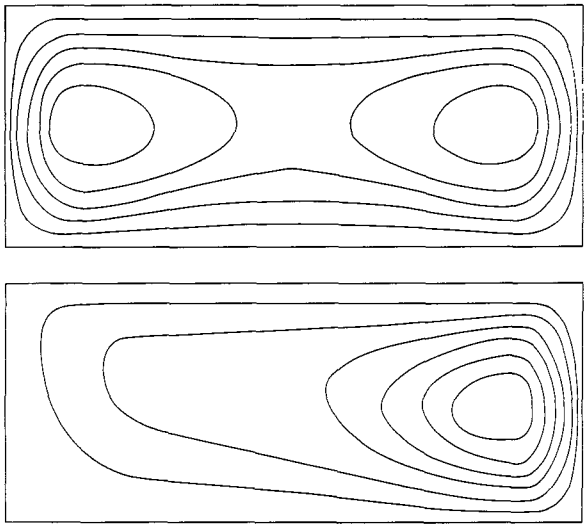

Figure 3. Contours of stream-function ψ for cells of width $\Delta = 2.4$. Top figure shows circulation driven by equally strong ascending and descending plumes. Lower figure shows circulation driven by a single descending plume.

The non-linear character of equation (15f) does not permit the coefficients B_n and D_n to be evaluated analytically. Instead, we set out in Section 6 a recursive algorithm with which they can be found.

As a preliminary illustration, contours of the stream-function with a surface plate present are shown in Fig. (3) for a cell with aspect ratio $\Delta = 2.4$.

Two cases are illustrated. In the upper diagram, the ascending and descending plumes have equal strength ($\gamma = 1/2$) and the stream-function is symmetrical about a vertical plane through the cell's midpoint. In the lower figure, there is only a descending plume ($\gamma = 0$) and its buoyancy causes the streamlines to crowd toward the right-hand side of the cell. Because of the surface plate, the velocity field, and hence the local heat transfer, is not the same along the upper and lower boundaries. This means that the interior temperature θ_i is not necessarily the average temperature of the two boundaries, and for the same reason the two plumes may not have the same strength. The two sets of contours in Fig. (3) represent the extremes in the range of possible plume strengths. In fact, we show in Section 6 that for all cell widths $0.2 \leqslant \Delta \leqslant 4.0$, the proper configuration has two plumes with nearly equal strength.

With the stream-function found, all that remains is to evaluate the Nusselt number, which will allow definite values of the stream-function to be assigned to the contours in Fig. (3).

Our approximation to the stream-function is weakest in the corners where the circulation is a Stokes flow only for very large values of R. This can be seen from the following dimensional arguments.

The equation of motion in the corners is, from equation (12),

$$\nabla^4 \psi = - R^{1/3} \frac{\partial \theta}{\partial X}.$$

If we denote by ϵ the length scale of the corner region, then in order of magnitude this becomes

$$\frac{\psi}{\epsilon^4} \sim \frac{R^{1/3}}{\epsilon}. \tag{17}$$

Since ψ increases by an amount $R^{-1/3}$ across the corners, equation (17) yields

$\epsilon \sim R^{-2/9}$.

Hence the corners contribute to the buoyancy force an amount $\epsilon^2 R^{1/3} = R^{-1/9}$. Recalling that the plumes' contribution to the buoyancy force is $O(1)$, it is clear that at finite Rayleigh numbers the corners may contribute to the driving force a small but non-negligible amount.

5 Plumes and thermal boundary layers

In this section the thermal boundary layers are analysed in order to relate the surface heat flux to the motion. The key requirement here is that the temperature field be periodic around the cell edges. Because of this periodicity requirement the easiest starting points are the plumes, which are most nearly self-similar.

The heat equation in the plumes is

$$\left(u\frac{\partial}{\partial X} + W\frac{\partial}{\partial Z} - 1/R^{2/3}\frac{\partial^2}{\partial X^2}\right)\theta = 0. \tag{18}$$

Also, from equation (7), we have the integral condition at $X = 0$

$$\int_0^\infty (\theta - \theta_i) W d\eta = \frac{\gamma Nu \Delta}{R^{1/3}} \tag{19}$$

where η is the boundary layer coordinate. Since W is, to $O(\delta_p)$, only a function of Z in the plume, equation (18) can be written as

$$\left(W\frac{\partial}{\partial Z} - XW'\frac{\partial}{\partial X} - 1/R^{2/3}\frac{\partial^2}{\partial X^2}\right)\theta = 0 \tag{20}$$

with $W' = \partial W/\partial Z$. We seek solutions to equation (20) of the form

$$\frac{\theta - \theta_i}{\theta_0(Z) - \theta_i} = f[X/\delta_p(Z)] = f(\eta) \tag{21}$$

where θ_0 is the temperature on the plume axis and η is scaled so that

$$\int_0^\infty f(\eta)\, d\eta = 1. \tag{22}$$

Substituting equation (21) into equation (20) yields

$$f'' + \lambda R^{2/3}(\eta f' + f) = 0, \tag{23}$$

λ a constant, plus an equation for the thickness:

$$\tfrac{1}{2}(\delta_p^2)' + \frac{W'}{W}\delta_p^2 - \lambda/W = 0. \tag{24}$$

Using the constraint (22), solutions to equations (23) and (24) are

$$f(\eta) = \exp(-\pi\eta^2/4), \tag{25}$$

$$\delta_p(Z) = \frac{1}{WR^{1/3}}\left[K_0 + \pi\int_0^Z W\, dZ'\right]^{1/2}, \tag{26}$$

K_0 being a constant of integration. The flux integral (19) can be applied to equation (26) at the plumes' $Z = 0$ to fix K_0:

$$K_0 = \frac{\gamma^2 \Delta^2 Nu^2}{(\theta_0^0 - \theta_i)^2 R^{2/3}} \tag{27}$$

where $\theta_0^0 = \theta$ $(X = 0, Z = 0)$. The first term in equation (26) represents a displacement thickness, the second a diffusion thickness. In this case they are of the same order of magnitude. Combining equations (19)–(26), the temperature along the plume axis ($X = 0$) is

$$\theta_0(Z) = \theta_i + \frac{\theta_0^0 - \theta_i}{[1 + \pi J(\theta_0^0 - \theta_i)^2 R^{2/3}/\gamma^2 \Delta^2 Nu^2]^{1/2}} \tag{28}$$

with

$$J = \int_0^Z W \, dZ'.$$

This result illustrates that temperature along the plume axis decreases only slowly with height, as anticipated in Section 3. For example, approximating W by $0.3\,(1 - Z)Z$, $Nu/R^{1/3}$ by 0.15, setting $\gamma = 0.5$, $\theta_i = 0$, and $\Delta = 2.0$, equation (28) yields

$$\frac{\theta_0(Z = 1)}{\theta_0^0} \simeq 0.6 \tag{29}$$

so that the central temperature in the plume is reduced only to about 60 per cent of its initial value before reaching the opposite surface.

The terminus of this plume forms the initial temperature profile for the boundary layers. Fig. (4) is a sketch of an ascending plume incident upon the upper surface $Z = 1$. It is useful to divide the upper surface into two segments, as shown. The segment $0 \leqslant X \leqslant X_1$ lies directly above the plume in the stagnation region and the heat flux there is controlled by the high temperatures of the plume. The appropriate heat equation is

$$\left(u \frac{\partial}{\partial X} + W \frac{\partial}{\partial Z} - 1/R^{2/3} \frac{\partial^2}{\partial Z^2}\right) \theta = 0 \tag{30}$$

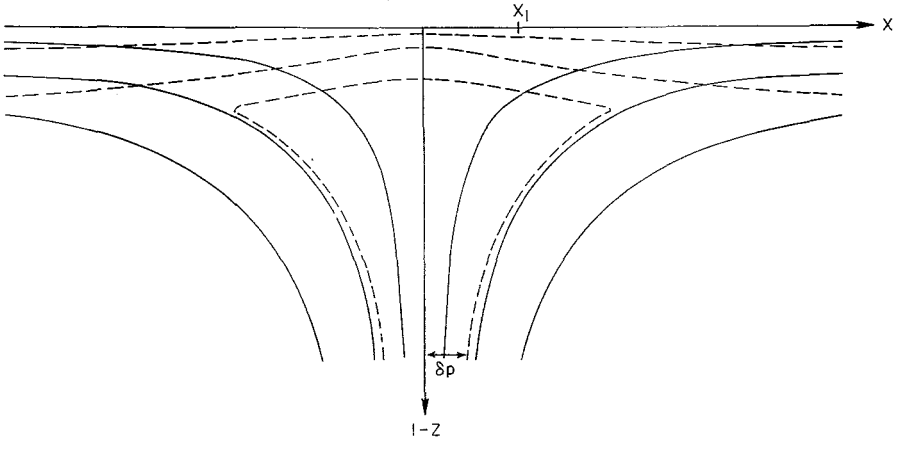

Figure 4. Sketch showing detail of thermal plume incident on upper surface: —— streamlines; – – – – isotherms: δ_p is plume (half) thickness.

subject to conditions

$$\begin{aligned} \theta &= -\tfrac{1}{2} \quad \text{on } \bar{Z} = 1 - Z = 0 \\ &= \theta_0(0) \quad \text{as } \bar{Z} \to 1, \end{aligned} \tag{31}$$

$\theta_0(0)$ defined by equation (28) evaluated at $\bar{Z} = 1 - Z = 0$. The solution to equations (30) and (31) is

$$\theta = -\tfrac{1}{2} + \frac{[\tfrac{1}{2} + \theta_0(0)]}{\sqrt{\pi}} \int_0^{\zeta} \exp(-\zeta'^2/4)\, d\zeta' \tag{32}$$

where

$$\zeta = 1/R^{2/3} \int_0^X u\, dX'.$$

The local Nusselt number is given by

$$\frac{Nu_l(X)}{R^{1/3}} = \frac{\tfrac{1}{2} + \theta_0(0)}{\sqrt{\pi}} \frac{u(X)}{\left[\int_0^X u\, dX'\right]^{1/2}}. \tag{33}$$

Beyond X_1, the accelerating flow draws the plume material into a horizontal sheet, so that the highest temperatures occur within the boundary layer rather than at its base. This behaviour is illustrated in Fig. (2). The first task is thus to construct a profile with these characteristics which can be used as initial data, and then follow the layer as it evolves downstream.

The portion of this initial profile due to the hot plume material, say θ_p, is just a continuation of the plume around the corner:

$$\theta_p = \theta_i + [\theta_0(0) - \theta_i)\, [\exp(-\pi\eta^2/4) - 1], \tag{34}$$

here

$$\eta = \frac{\bar{Z}u(X_1)\, [\theta_0(0) - \theta_i]\, R^{2/3}}{\gamma \Delta Nu}. \tag{35}$$

The remaining part is the contribution from the boundary layer above the plume, given by equation (32). Equations (32) and (34) give in combination the composite profile at X_1:

$$\theta_c = [\theta_0(0) - \theta_i]\ [\exp(-\pi\eta^2/4) - 1] - \tfrac{1}{2} + \frac{[\tfrac{1}{2} + \theta_0(0)]}{\sqrt{\pi}} \int_0^{\zeta} \exp(-\zeta'^2/4)\, d\zeta'. \tag{36}$$

The boundary layer can now be evaluated over the segment $X_1 \leqslant X \leqslant \Delta$ by solving equation (30) subject to the conditions

$$\begin{aligned} \theta &= -\tfrac{1}{2} \quad \text{on } \bar{Z} = 0 \\ &\to \theta_i \quad \text{as } \bar{Z} \to 1 \\ &= \theta_c \quad \text{on } X = X_1. \end{aligned} \tag{37}$$

Equation (30) can be transformed into a standard one-dimensional heat equation with the help of the Von Mises transformation. In terms of new independent variables (ζ_1, ψ), where

$$\zeta_1 = 1/R^{2/3} \int_{X_1}^X u\, dX',$$

and ψ is the stream-function, it is

$$\frac{\partial\theta}{\partial\zeta_1}=\frac{\partial^2\theta}{\partial\psi^2} \tag{38}$$

using conventional methods (e.g. Carslaw & Jaeger 1959, p. 357) the solution to equations (37) and (38) is

$$\theta-\theta_i=\left(\frac{1}{4\pi\zeta_1}\right)^{1/2}\int_0^\infty[\theta_c(\psi')-\theta_i]\{\exp-(\psi-\psi')^2/4\zeta_1-\exp-(\psi+\psi')^2/4\zeta_1\}\,d\psi'$$
$$-(\tfrac{1}{2}+\theta_i)\operatorname{erfc}(\psi/2\sqrt{\zeta_1}) \tag{39}$$

and the local heat flux is given by

$$\frac{Nu_l}{R^{1/3}}=\frac{2}{\pi}[\tfrac{1}{2}+\theta_0(0)]h\int_0^\infty\exp\left[-\eta^2\left(\frac{h^2}{k^2}+1\right)\right]d\eta-2\sqrt{\pi}[\theta_0(0)-\theta_i]\frac{l^2}{k}$$
$$\times\int_0^\infty\eta\exp\left[-\eta^2\left(\frac{\pi l^2}{k^2}+1\right)\right]d\eta \tag{40}$$

where

$$h(X_1)=u(X_1)\Big/\left[\int_0^{X_1}u\,dX'\right]^{1/2},$$

$$l(X_1)=[\theta_0(0)-\theta_i]R^{1/3}u(X_1)/\gamma\Delta Nu,$$

$$k(X,X_1)=u(X)\Big/\left[\int_{X_1}^{X}u\,dX'\right]^{1/2},$$

$$\eta=\psi/2\sqrt{\zeta_1}.$$

The expression for the heat flux (equation 40) becomes simpler in two limits: at $X=X_1$ it is

$$\frac{\tfrac{1}{2}+\theta_0(0)}{\sqrt{\pi}}\,\frac{u(X_1)}{\left[\int_0^{X_1}u\,dX'\right]^{1/2}}$$

in agreement with equation (33). At the other extreme, as $X\to\infty$, equation (40) becomes

$$\frac{\tfrac{1}{2}+\theta_i}{\sqrt{\pi}}\,\frac{u}{\left[\int_{X_1}^{X}u\,dX'\right]^{1/2}}$$

which is the heat transfer from a self-similar boundary layer and indicates that the temperature profile achieves similarity at extreme distances from the hot plume, as anticipated at the beginning of this section.

The total heat flux from the layer is

$$\Delta Nu=\int_0^\Delta Nu_l(X)\,dX \tag{41}$$

the integrand being expression (33) for $0\leqslant X\leqslant X_1$, and expression (40) for $X_1\leqslant X\leqslant\Delta$.

6 Matching solutions

In Sections 4 and 5 the stream-function and temperature field for the interior and the boundary layers, respectively, have been determined to within constant factors. In this section these two solutions are matched. To accomplish this it is necessary to find a coefficient for the stream-function ψ, the value of the interior temperature θ_i, and values for the plume strength γ which equate the heat transfer in the plumes (equation 15f) and in the boundary layers (equation 41). There exist two additional constraints, as yet not used, which make this possible.

First, heat must leave the system at the same rate it enters, or

$$Nu(Z = 0) = Nu(Z = 1). \tag{42}$$

A second constraint is on temperature in the cell interior. If U_b and θ_b denote velocity and temperature along the streamline which bounds the cell, and dl denotes a segment of that streamline, then the interior temperature is

$$\theta_i = \frac{\oint \theta_b U_b \, dl}{\oint U_b \, dl} \tag{43}$$

This result is derived in Corcos & Olson (1980).

The following sequence of steps allows ψ and Nu to be found, subject to constraints (42) and (43), plus the requirement that the heat flux computed by equations (41) and (15f) be equal.

First, choose a value for γ and set

$$-\gamma = \frac{\partial^2 \psi}{\partial X^2} \frac{\partial \psi}{\partial X}\bigg|_{X=0},$$

$0 \leqslant \gamma \leqslant 1$, which means

$$1 - \gamma = \frac{\partial^2 \psi}{\partial X^2} \frac{\partial \psi}{\partial X}\bigg|_{X=\Delta}.$$

Then the non-linear condition (15f) can be enforced, to within a constant multiple, by forming an iterative sequence of functions ψ^m, $m = 1 \ldots M$ of the form given by equation (16) and subject to

$$\begin{aligned} \frac{\partial^2 \psi^1}{\partial X^2}\bigg|_{0,\Delta} &= (-\gamma, 1-\gamma), \quad m = 1 \\ \frac{\partial^2 \psi^m}{\partial X^2}\bigg|_{0,\Delta} &= (-\gamma, 1-\gamma)\left(\frac{\partial \psi^{m-1}}{\partial X}\bigg|_{0,\Delta}\right)^{-1}, \quad m > 1. \end{aligned} \tag{44}$$

Summing the series (16) to $N = 30$ produces a stream-function everywhere convergent to within 0.1 per cent; application of the iterative sequence (44) to $M = 5$, using trapezoidal rule integration over 35 points, makes the products

$$\frac{\partial^2 \psi}{\partial X^2} \frac{\partial \psi}{\partial X}\bigg|_{0,\Delta}$$

constant to within 2 per cent at all points Z. Next, provisional values of Nu for top and bottom boundaries can be computed using ψ^M in equation (41) with θ_i set to zero. The integrals (33), (40) and (41) were evaluated using the trapezoidal rule over unequally spaced points. Convergence to 0.1 per cent was obtained with 35 points in X and 20 in Z. We denote by $\widehat{Nu}(0)$, $\widehat{Nu}(1)$ the values obtained this way. Condition (42) is then met by requiring the interior temperature to be

$$\theta_i(\gamma, \Delta) = \frac{\frac{1}{2}[\widehat{Nu}(0) - \widehat{Nu}(1)]}{\widehat{Nu}(0) + \widehat{Nu}(1)} \tag{45}$$

in which case the value of Nu, top and bottom, resulting from equation (45) becomes

$$E = \frac{2\widehat{Nu}(0)\widehat{Nu}(1)}{\widehat{Nu}(0) + \widehat{Nu}(1)}. \tag{46}$$

Finally, the stream-function can be rescaled to make plume and boundary layer heat transfers equal. Multiplying the stream-function ψ^M by a constant C makes the plume heat flux, given by equation (44), equal to C^2, while the heat flux through the boundary layers becomes $C^{1/2}E$ (by equations 40 and 46). Equating these two fluxes yields

$$C = E^{2/3}$$

so

$$\begin{aligned} \psi(\gamma, \Delta) &= C\psi^M = E^{2/3}R^{-2/9}\psi^M \\ Nu(\gamma, \Delta) &= C^{1/2}E = E^{4/3}R^{-1/9}. \end{aligned} \tag{47}$$

We now use the constraint (43) to find the proper value of γ. For the case of a homogeneous layer, by symmetry $\gamma = 1/2$ and $\theta_i = 0$. For the case of a surface plate $\theta_i \neq 0$ necessarily, but we have two constraints on θ_i, namely equations (43) and (45). These constraints are compatible only for the correct value of the plume strength γ. In general it is necessary to compute, $\psi(\gamma, \Delta)$ and $\theta_i(\gamma, \Delta)$ over a range of values γ to find the intersection of the curves (43) and (45). We found that $0.5 \leqslant \gamma \leqslant 0.52$ and $0 \leqslant \theta_i \leqslant 0.02$ for all cells $0.2 \leqslant \Delta \leqslant 4.0$. The *a priori* assumption that the interior temperature is the mean of the boundary temperatures, while not precisely correct, results in a negligible error.

The computation outlined in this section has been carried out for cells of width $0.2 \leqslant \Delta \leqslant 4.0$ and results are presented in the following section. Computations for one cell require less than 5 s of CPU time on a DEC-10 computer.

7 Discussion of results

Using the methods outlined in the preceding three sections, we have determined the field of motion and thermal structure for convection in cells with different aspect ratios Δ. We exhibit results for a homogeneous layer with free surfaces and for a layer with surface plates. In all cases the heat is supplied from below. Figs (5)–(9) illustrate results for convection with plates; these will be discussed first.

Fig. (5) shows the variation of Nusselt number and plate speed with cell width. There is a maximum heat transfer at $\Delta = 0.8$, and for long cells $Nu \sim \Delta^{-2/3}$. The maximum plate speed occurs at $\Delta = 1.8$ and decreases as $U \sim \Delta^{-1/6}$ for elongate cells. It has been argued heuristically (Malkus & Veronis 1958) that at finite amplitude the stable configuration is the one which maximizes the heat transfer. Certainly more considerations than just heat

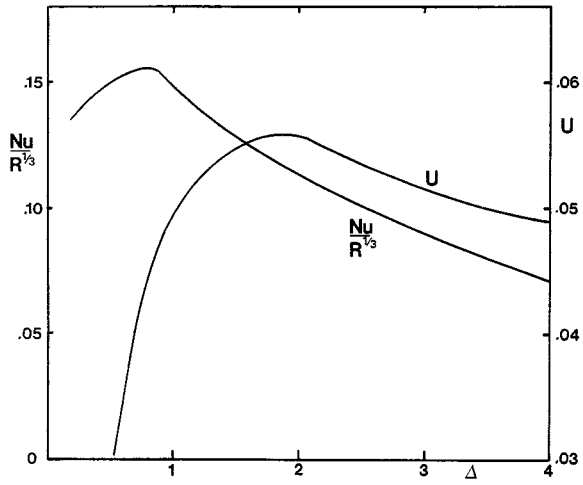

Figure 5. Non-dimensional surface heat flux and plate speed as a function of cell width Δ, for heat supplied from below. Scaling for plate speed V is as in Table 1.

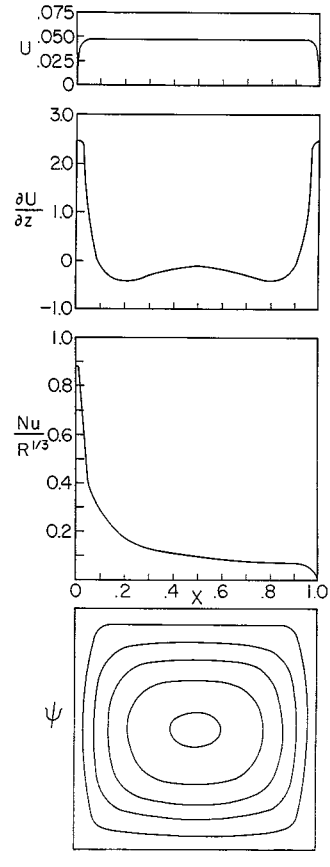

Figure 6

Figures 6–8. Non-dimensional plate speed, shear stress on plate, surface heat flux and stream-function contours for cells of widths Δ = 1, 2, 3, driven by heat from below. Scaling is as in Table 1.

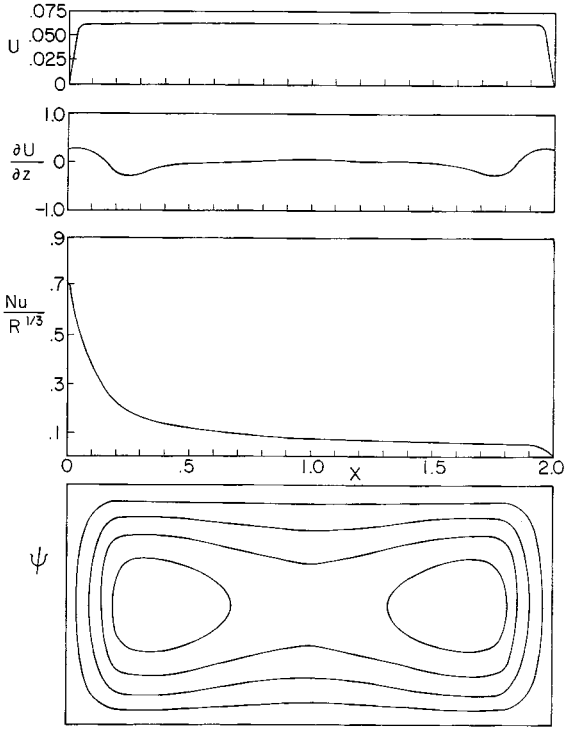

Figure 7

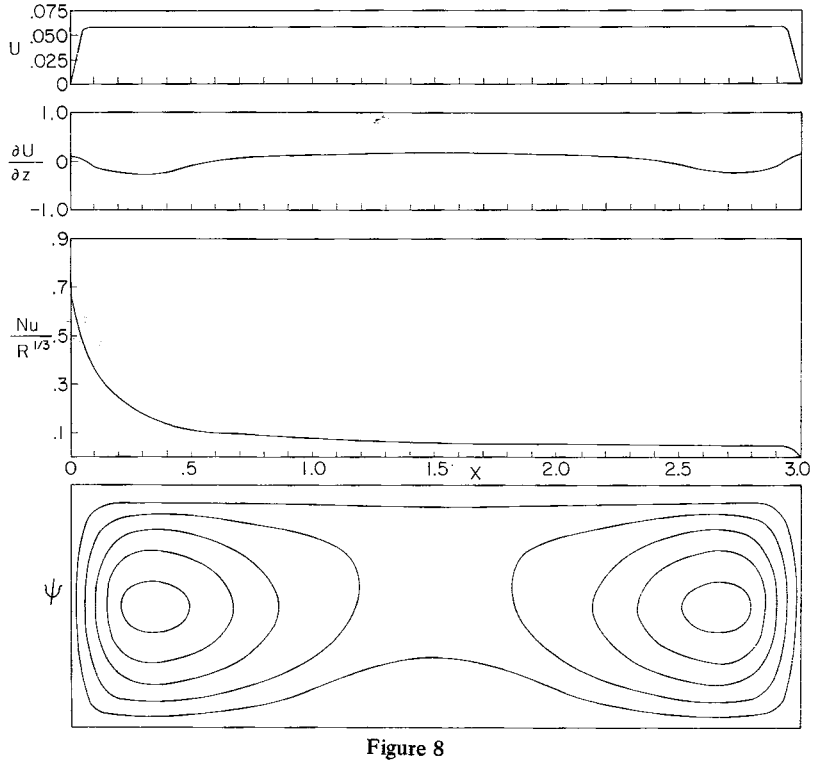

Figure 8

Table 1.

	Quantity	Scaling
Position	$\mathbf{X}$	$D\mathbf{X}^*$
Stream-function	ψ	$kR^{2/3}\psi^*$
Velocity	$\mathbf{u}$	$(kR^{2/3}/D)\mathbf{u}^*$
Shear stress	$\mu\partial u/\partial Z$	$(\mu kR^{2/3}/D^2)\partial u^*/\partial Z^*$
Temperature	T, θ	$\Delta T(T^*, \theta^*)$; $\Delta T = T_0 - T_1$
Heat flux	q	$K\Delta TNu/D$
Plate length	L	$D\Delta$

Table 2.

	Quantity	Adopted value
Mantle viscosity	μ	10^{22} poise
Thermal conductivity	K	2.5×10^5 erg cm^{-1} deg^{-1}
Thermal diffusivity	k	6×10^{-3} cm^2 s^{-1}
Temperature scale height	$C_p/\alpha g$	10 000 km
Mean mantle heat flux	q	55 erg cm^{-2} s^{-1}
Mean plate speed	V	1.25×10^{-7} cm s^{-1} (4 cm yr^{-1})
Mean plate length	L	6900 km
Depth of convecting layer	D	2900 km

transfer enter into determining stable configurations (*cf.* Busse 1967) but as we show later, this behaviour serves as a rough guide.

Figs (6)–(8) show calculable quantities for cells of widths 1, 2 and 3 respectively. The stream-function, surface heat flux, plate speed and shear stress on the plate are all shown in terms of scaled variables. For converting to dimensional quantities, Table 1 gives the scaling used in each case.

The most noticeable feature of the stream-function is the development of a broad velocity minimum, in the mid-region of the cell, as the width increases. At $\Delta = 3$ it is likely that only the stabilizing influence of the plate prevents development of three distinct circulations. Fig. (9) shows the detailed boundary layer structure along the lower boundary for a plate of length $\Delta = 4$. The vertical scale measures the boundary layer coordinate and is stretched out for emphasis. The bulge in the isotherms represents a source of vorticity for any finite value of R, and is likely to be the seat of instability.

Some information on stability can be gotten from the boundary layers, since for these steady solutions to be stable, their boundary layers must be stable. The stability of the thermal layers depends on a local Rayleigh number, R_δ, which can be expressed in terms of the global Rayleigh number, the boundary layer thickness and the cell depth:

$$R_\delta = \frac{R}{2}\left(\frac{\delta}{D}\right)^3.$$

Since $\delta/D \propto R^{-1/3}$, R_δ is independent of R and is a function only of position X and cell width Δ. Fig. (14) shows the dependence of R_δ on Δ at the point $X = \Delta/2$ for the lower thermal layer. The layer will be stable only for $R_\delta \leqq 10^3$, so the results in Fig. (14) imply that the *lower* boundary layer is unstable for both elongate ($\Delta \gg 1$) and narrow ($\Delta \ll 1$) cells.

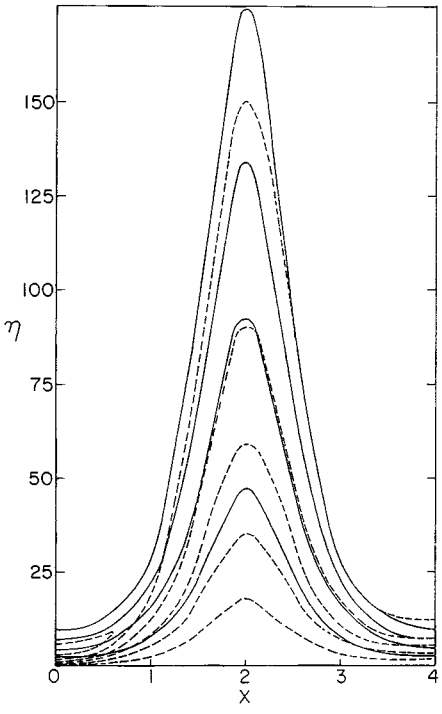

Figure 9. Streamlines —— and isotherms – – – – within lower boundary layer for cell of width $\Delta = 4$ driven by heat from below. Horizontal scale is non-dimensional coordinate X, vertical scale is non-dimensional boundary layer coordinate $\eta = ZR^{1/3}$. This illustrates development of an incipient plume off the lower free surface. Flow is left to right.

Figs (5)–(8) indicate that the plate speed is not very sensitive to the cell length. Comparing the plate speeds obtained here with results from similar calculations carried out with a *free* upper boundary (see Fig. 10), the plate surface translates with a speed which is roughly the mean velocity at a free boundary.

Shear stresses on the plate are nowhere very large (with a viscosity of 10^{22} poise, all stresses in Figs (6)–(8) are less than 40 bars) although the computed values where the plumes form are probably not too reliable since the motion there is not a Stokes flow. It is enough to note that the plates are under tension near upwelling plumes (ridges), are under compression near descending plumes (trenches) and are subject to only small stresses in between.

Fig. (10) shows the variation of *Nu* and mean surface velocity for the case of a homogeneous layer with stress-free surfaces. The Nusselt numbers shown here are about 20 per cent lower than those computed at finite R using grid methods (see Moore & Weiss 1973, for example). We attribute this discrepancy to effects at finite values of R which are felt most strongly in the corner regions, and where the convergence of our method is the slowest.

A stated purpose of this calculation is to compare the speed of plates driven by thermal convection with observed rates of seafloor spreading. Formula (6) is convenient as it expresses the plate speed in terms of several parameters for which independent geophysical measurements exist (Elsasser *et al.* 1979), plus the convecting layer depth. There is still no agreement among geophysicists on the question of how deep convective motion penetrates into the mantle, although only two hypotheses are widely discussed: convection limited to

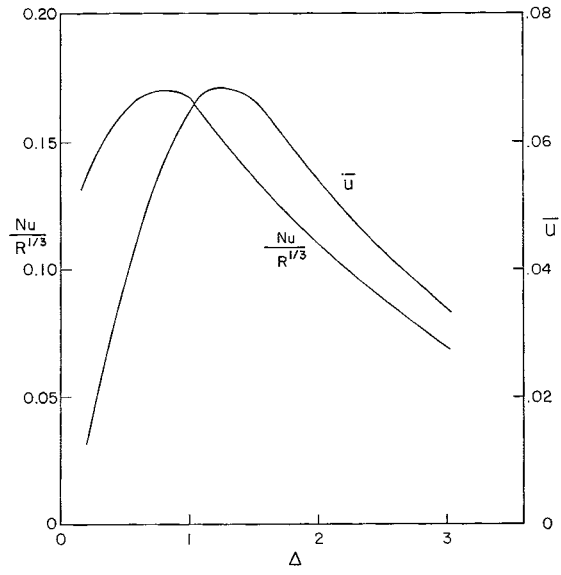

Figure 10. Non-dimensional average surface heat flux and average surface velocity as a function of cell width, for Rayleigh–Bénard convection.

the mantle's upper 600–700 km and convection extending all the way to the mantle's base. Here, we will adopt these two values as representative limits. To evaluate equation (6), we take $\mu = 10^{22}$ P, $L = 6900$ km as an average plate length (which implies $\Delta \simeq 2.4$ for $D = 2900$ and $\Delta \simeq 10$ for $D = 700$), $q = 55$ mW m^{-2} as an average mantle heat flux, $\sqrt{C_p/\alpha g} \simeq 3.2 \times 10^4$ cm$^{1/2}$ as a mean value computed from earth model 1066B of Gilbert & Dziewonski (1975) using methods of either Verhoogen (1951) or Stacey (1977). (Table 2 gives values of parameters adopted in this calculation.)

With these values plus the values of $a_1(\Delta)$ and $a_2(\Delta)$ from Fig. (5) (which are extrapolated to $\Delta = 10$ for $D = 700$ km), formula (6) predicts a mean plate speed of about 1 cm yr^{-1} for a 700 km deep convecting layer and about 4 cm yr^{-1} for convection extending through the whole mantle. Some estimates of mean plate speeds are 3.6 cm yr^{-1} (Forsyth & Uyeda 1975) and 4.4 cm yr^{-1} (Solomon & Sleep 1974). Thus we conclude that from what is known about the mantle's behaviour, thermal convection, especially whole mantle convection, is marginally able to account for the observed plate speeds. We say 'marginally' to emphasize that this conclusion is based on a highly idealized model of mantle convection; our system is steady, two-dimensional with constant transport properties and for example does not include a very faithful representation of the subduction process. Also, the same calculation done with motions driven by internal heating would yield somewhat smaller velocities than those calculated here for cells heated from below. In spite of all these deficiencies it is still gratifying that such a simple model can account for the observed plate speeds without violating crucial observational constraints such as surface heat flow and mantle viscosity and without relying on external, unspecified sources of energy.

Results from a specific case can now be compared with some existing data. Because deep mantle convection involves cells of reasonable aspect ratio, we take the cell depth to be 2900 km and consider a plate 6900 km long, which is representative of plate dimensions. We adopt a value of 10^{22} P for the viscosity and fix the plate speed at 4 cm yr^{-1}. By choosing these parameters, all others are specified. Contours of the stream-function in this case are the same as in Fig. (3). Fig. (11) shows the surface heat flux as a function of age, with data

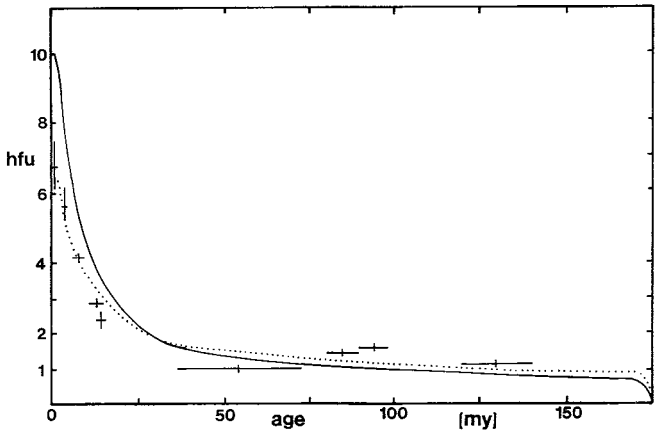

Figure 11. Surface heat flow, in hfu = μ cal cm^{-2} s^{-1}, versus age along a plate of length 6900 km moving at 4 cm yr^{-1}. —— Heat from below; ..... similarity profile; —|— data for North Pacific from Parsons & Sclater (1977).

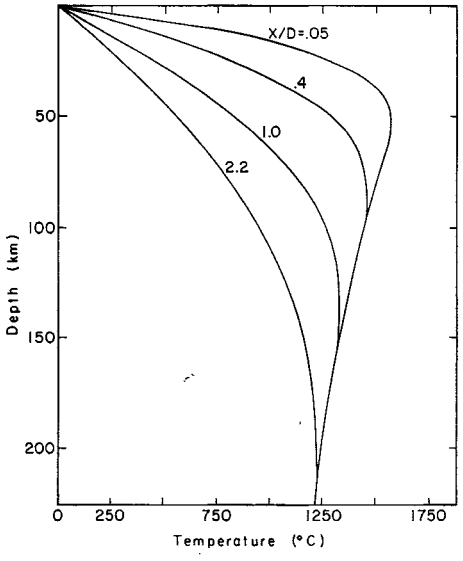

Figure 12. Near surface geotherms taken at various distances X along a plate of length ΔD = 6900 km, Δ = 2.4, moving at 4 cm yr^{-1}, driven by heat from below. Included is an adiabatic increase of 0.3 deg km^{-1}. Note the local maximum at depths of 50–150 km.

from the North Pacific (Parsons & Sclater 1977) included for comparison. There is fair agreement everywhere except immediately at the ridge crest, where local effects must be taken into account (Yuen, Tovish & Schubert 1978). Fig. (12) shows a sequence of geotherms at various intervals between ridge and trench. These include an adiabatic gradient of 0.3 deg km^{-1}. As a result of the hot rising plume, the temperature profile develops a local maximum which is most shallow and pronounced near the ridge and gradually diminishes and recedes from the surface with increasing age. It is widely believed that low seismic velocities and low Q values observed at depths of 50–150 km are due to high temperatures (Anderson & Minster 1979) and that this zone defines the asthenosphere. The present study indicates that the existence of an asthenosphere could be a consequence of large scale

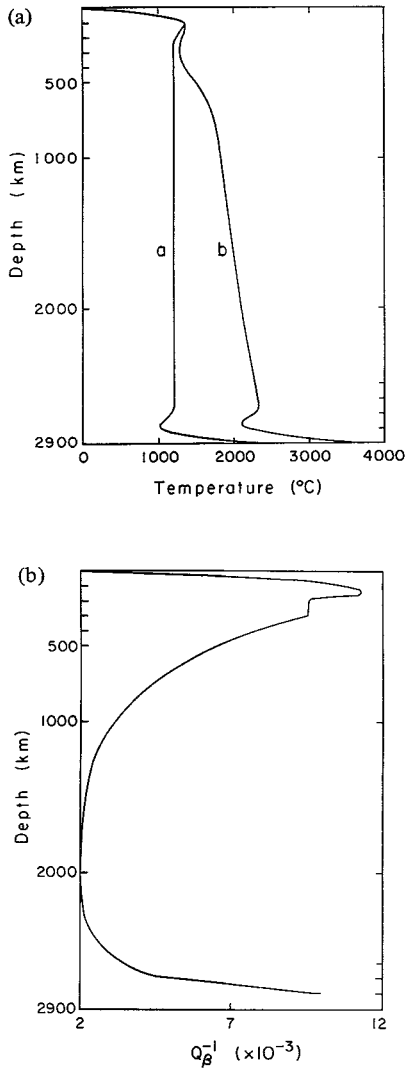

Figure 13. (a) Laterally averaged mantle geotherms: curve a is profile calculated with Boussinesq approximation; b is as a, with 200°C increase across phase transitions and adiabat added on. (b) Profile of shear wave attenuation, expressed as Q_β^{-1} from Anderson & Hart (1978).

convection and not a cause, and its depth is defined by a local maximum in the boundary layer geotherm. Admittedly the situation illustrated by Fig. (12) represents an extreme case in which all heating comes from below; the maxima become less pronounced as a greater fraction of the heat is produced internally. However, while it is likely that mantle radioactivity supplies much of the internal energy to drive the flow, recent work on the dynamo (Busse 1975; Loper 1978) suggests that a measurable fraction of the observed surface heat flux is extracted by the mantle from the core, and so it is at least plausible that these local geotherm maxima exist.

Finally, Fig. 13(a) represents horizontally averaged geotherms through the mantle. Curve a is the temperature profile calculated using the Boussinesq approximation. Curve b is the same profile with adiabatic increases added on, including a 200°C increase across the phase

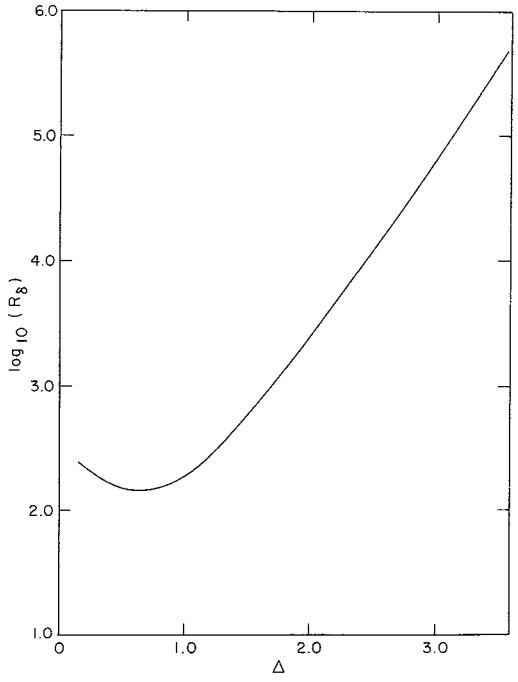

Figure 14. Maximum Rayleigh number of lower thermal layer, versus cell width Δ.

transition region centred at 500 km depth. The adiabatic gradient has been calculated using data from earth model 1066B. It is interesting to note how similar in form the geotherm with upper and lower thermal layers is to recent estimates of mantle shear wave attenuation. Fig. 13(b) shows for comparison the distribution of Q_β^{-1} from model (SL8) of Anderson & Hart (1978). This similarity suggests that a plausible interpretation of the observed high attenuation at the base of the mantle is that it is due to a hot thermal boundary layer.

8 Conclusions

We have analysed the fine structure of steady, two-dimensional thermal convection with moving surface plates using boundary layer methods. The analysis reveals several distinctive properties of thermal convection which are relevant to the question of driving forces for plate motions.

For a layer heated from below, steady solutions were found for all cell sizes Δ. With a surface plate, the heat flux reaches a maximum at $\Delta = 0.8$ and decreases as $\Delta^{-2/3}$ for $\Delta > 1$. The drift speed of a surface plate was found to be not very sensitive to its length, decreasing only slightly with increasing length, and having a maximum at $\Delta = 1.8$. For a homogeneous layer with free surfaces (the Rayleigh–Bénard case), the heat flux is maximum at $\Delta = 0.7$ and decreases as Δ^{-1} for elongate cells.

By scaling our results and using published values for global heat flow and mantle viscosity, we find that steady convection driven by heat from below can move plates at about 1 or 4 cm yr^{-1} if the depth of circulation is 700 or 2900 km, respectively. In all cases, local stresses on drifting plates are small except near leading and trailing edges which are under compression and tension, respectively.

If a significant amount of the heat which drives the motion comes from below the convecting domain, then there should be a hot thermal boundary layer at its base and a cold one at its top. The boundary layers have a complex structure which includes, in the case of

the upper cold one, a local interior maximum in the temperature profile. Scaled to mantle conditions, this maximum should occur at depths of 50–150 km which suggests that it might define the depth to the low-velocity zone.

Acknowledgments

This research was partially supported by the National Science Foundation under grants EAR-7904823 and ENG-7806884.

References

Anderson, D. L. & Hart, R. S., 1978. *Q* of the earth, *J. geophys. Res.*, **83**, 5869–5882.

Anderson, D. L. & Minster, J. B., 1979. Seismic velocity, attenuation and rheology of the upper mantle, *Phys. Earth planet. Interiors*, J. Coulomb Symposium.

Busse, F. H., 1967. On the stability of two-dimensional convection in a layer heated from below, *J. math. Phys.*, **46**, 140–150.

Busse, F. H., 1975. A model of the geodynamo, *Geophys. J. R. astr. Soc.*, **42**, 437–459.

Carslaw, H. S. & Jaeger, J. C., 1959. *Conduction of Heat in Solids*, 2nd ed., Clarendon Press, Oxford.

Corcos, G. M. & Olson, P., 1980. Steady cellular two-dimensional convection at infinite Prandtl and large Rayleigh numbers, to appear.

Elsasser, W. M., Olson, P. & Marsh, B. D., 1979. The depth of mantle convection, *J. geophys. Res.*, **84**, 147–155.

Forsyth, D. & Uyeda, S., 1975. On the relative importance of the driving forces of plate motion, *Geophys. J. R. astr. Soc.*, **43**, 163–200.

Gilbert, F. & Dziewonski, A., 1975. An application of normal mode theory to the retrieval of structural parameters and source mechanisms from seismic spectra, *Phil. Trans. R. Soc. Lond.*, **A278**, 187–269.

Houston, M. H. Jr, & DeBremacker, J-Cl., 1975. Numerical models of convection in the upper mantle, *J. geophys. Res.*, **80**, 742–751.

Loper, D. E., 1978. The gravitationally powered dynamo, *Geophys. J. R. astr. Soc.*, **54**, 389–404.

Lux, R. A., Davies, G. F. & Thomas, J. H., 1979. Moving lithospheric plates and mantle convection, *Geophys. J. R. astr. Soc.*, **58**, 209–228.

Malkus, W. M. & Veronis, G., 1958. Finite amplitude cellular convection, *J. Fluid Mech.*, **4**, 225–260.

McKenzie, D. P., Roberts, J. M. & Weiss, N. O., 1974. Convection in the earth's mantle: towards a numerical simulation, *J. Fluid Mech.*, **62**, 465–538.

Moore, D. R. & Weiss, N. O., 1973. Two-dimensional Rayleigh–Bénard convection, *J. Fluid Mech.*, **58**, 289–312.

Parmentier, E. M. & Turcotte, D. L., 1978. Two dimensional mantle flow beneath a rigid accreting lithosphere, *Phys. Earth planet. Interiors*, **17**, 281–289.

Parsons, B. & Sclater, J. G., 1977. An analysis of the variation of ocean floor heat flow and bathymetry with age, *J. geophys. Res.*, **82**, 803–827.

Roberts, G. O., 1979. Fast viscous Bénard convection, *Geophys. Astrophys. Fluid Dynamics*, **12**, 235–272.

Roberts, G. O., 1977. Fast viscous convection, *Geophys. Astrophys. Fluid Dynamics*, **8**, 197–233.

Robinson, J. L., 1967. Finite amplitude convection cells, *J. Fluid Mech.*, **30**, 577–600.

Schubert, G. & Young, R. E., 1976. Cooling of the earth by whole-mantle subsolidus convection: a constraint on the viscosity of the lower mantle, *Tectonophysics*, **35**, 201–214.

Solomon, S. C. & Sleep, N. H., 1974. Some simple physical models for absolute plate motions, *J. geophys. Res.*, **79**, 2557.

Stacey, F. D., 1977. A thermal model of the earth, *Phys. Earth planet. Interiors*, **15**, 341–348.

Turcotte, D. L., Hsiu, A. T., Torrance, K. E. & Schubert, G., 1974. Influence of viscous dissipation on Bénard convection, *J. Fluid Mech.*, **64**, 369–374.

Turcotte, D. L., 1967. A boundary layer theory for cellular convection, *Int. J. Heat Mass Transfer*, **10**, 1065–1074.

Turcotte, D. L. & Oxburgh, R. E., 1967. Finite amplitude convection cells and continental drift, *J. Fluid Mech.*, **28**, 29–42.

Verhoogen, J., 1951. The adiabatic gradient in the mantle, *Trans. Am. geophys. Un.*, **32**, 41–43.

Yuen, D. A., Tovish, A. & Schubert, A., 1978. Shear flow beneath oceanic plates: local nonsimilarity boundary layers for olivine rheology, *J. geophys. Res.*, **83**, 759–765.